https://doi.org/10.1016/j.jpowsour.2023.233057

Development and Performance Evaluation of a Passive Direct Ammonia Fuel Cell

Yun Liu[a], Zhefei Pan[a], Oladapo Christopher Esan[a], Xiaoyu Huo[a], Xingyi Shi[a], Liang An[a,*]

[a] Department of Mechanical Engineering, The Hong Kong Polytechnic University, Hung Hom, Kowloon, Hong Kong SAR, China

*Corresponding author.

Email: liang.an@polyu.edu.hk (L. An)

Abstract:

In this work, a new passive ammonia fuel cell prototype is designed and tested. The developed ammonia fuel cell features a passive supply of ammonia to the anode, eliminating the need for a complex fuel delivery system, while the cathode is designed as an open cathode to directly use oxygen from the ambient air as oxidant. To demonstrate the working principle of the passive ammonia fuel cell, its general performance is first investigated and results show that the developed passive ammonia fuel cell can provide a peak power density of 31.9 mW cm^{-2} and an open-circuit voltage of 0.63 V. To gain insights into the physical and chemical processes involved in the cell and as well enhance the understanding of the mass/charge transport mechanism within the cell, the developed passive ammonia fuel cell prototype was tested under different operating conditions, such as various operating temperature and reactant concentrations. In addition, the structural parameters of the membrane electrode assembly, such as the thickness of the membrane, catalyst loading, and hydrophobicity of the diffusion layer are investigated and analyzed to examine their influence on the mass transport behavior and performance of the passive ammonia fuel cell.

Key words

Ammonia; fuel cells; liquid fuel; hydrogen carrier; open cathode; anion exchange membrane

1. Introduction

Ammonia is a carbon-free and hydrogen-rich energy carrier (17.65 wt. %) with high bulk energy density (12.7 MJ/L) [1]. In addition, ammonia is easy to store (liquefied at -33.34 °C under ambient pressure), transport and handle, thus reducing operational costs. Besides, ammonia has well established storage and transport infrastructure worldwide. These compelling characteristics make ammonia a promising energy carrier [2]. Existing energy conversion technologies for converting ammonia to other energy sources include direct combustion of ammonia, hydrogen production from ammonia cracking, and ammonia fuel cells [3–5]. Among them, ammonia fuel cells, which is also free of carbon emissions, gain preference due to the fact that their products are only nitrogen and water [6]. Typical ammonia fuel cells can be divided into two categories, direct ammonia fuel cells and indirect ammonia fuel cells [7]. Indirect ammonia fuel cells, as the name implies, first crack ammonia into hydrogen and nitrogen (where ammonia is the hydrogen carrier) and then use the obtained hydrogen, after separation and purification, to generate electricity in a proton exchange membrane fuel cell [8,9]. In contrast, direct ammonia fuel cells use ammonia directly as a fuel and convert the chemical energy in ammonia into electrical energy through an electrochemical reaction, e.g., low temperature direct ammonia fuel cells, ammonia fed solid oxide fuel cells, etc. The advantage of direct ammonia fuel cells is that the chemical energy in ammonia can be converted directly into electrical energy, reducing the complexity of the reaction system compared to indirect ammonia fuel cells [10,11]. However, the development of direct ammonia fuel cells, especially low temperature direct ammonia fuel cells, is still facing some daunting challenges. Firstly, the sluggish reaction kinetics of ammonia oxidation at room temperature leads to low performance of direct ammonia fuel cells. In addition, the ammonia oxidation process may generate nitrogen-containing intermediate sorbents which poison the electrocatalysts [12]. To

enhance the performance of direct ammonia fuel cells, a number of representative research works have been conducted by researchers in recent years, enabling the performance improvement of direct ammonia fuel cells [13–16]. For example, in 2018, Gottesfeld et al. [17] developed an alkaline membrane direct ammonia fuel cell with a power density of 420 mW cm^{-2} at 100 °C. In 2019, a direct ammonia fuel cell developed by the Yushan Yan's group at The University of Delaware achieved a peak power density of 135 mW cm^{-2} at 80 °C. The performance of the direct ammonia fuel cell was further improved to 314 mW cm^{-2} [17] and 410 mW cm^{-2} [18] by modifying and improving the fuel cell anode electrocatalyst and cathode electrocatalyst, respectively. In addition, the application of non-precious metal catalysts in the design and operation of direct ammonia fuel cells has been investigated by Tao et. al [19,20]. In our previous work, we investigated the mass/charge transfer mechanism within the direct ammonia fuel cell and the effect of operating conditions on the performance of the direct ammonia fuel cell [21]. All these aforementioned studies have contributed to the enhancement of the performance of direct ammonia fuel cells and understanding of the reaction mechanism of these fuel cells. However, these direct ammonia fuel cell systems are all based on active fuel and oxidant supply systems. In other words, the fuel cells require the design of additional supply systems, which would limit the application of direct ammonia fuel cells in some specific applications, such as powering small portable devices. Therefore, a number of passive or self-breathing fuel cell configurations have received the interest of researchers in recent years [22–24]. These passive fuel cells are typically characterized by a single injection of fuel into the fuel cell anode compartment (without a peristaltic pump) and by diffusion from the anode flow field to the anode catalyst layer (ACL) where oxidation takes place. The corresponding oxidant, e.g., oxygen, is typically obtained directly from the air and is then transferred by diffusion from the cathode flow field to the cathode catalyst layer (CCL) where the

reduction reaction takes place. In addition, the mass transfer mechanism within the fuel cell deserves further investigation due to the change in the supply of fuel and oxidant. Following these considerations, this work develops a new passive ammonia fuel cell prototype, explores the reaction mechanism of passive ammonia fuel cells, broadens the application scenarios of ammonia fuel cells and further enhances the understanding of the role of direct ammonia fuel cell technology in renewable energy conversion.

2. Working principle

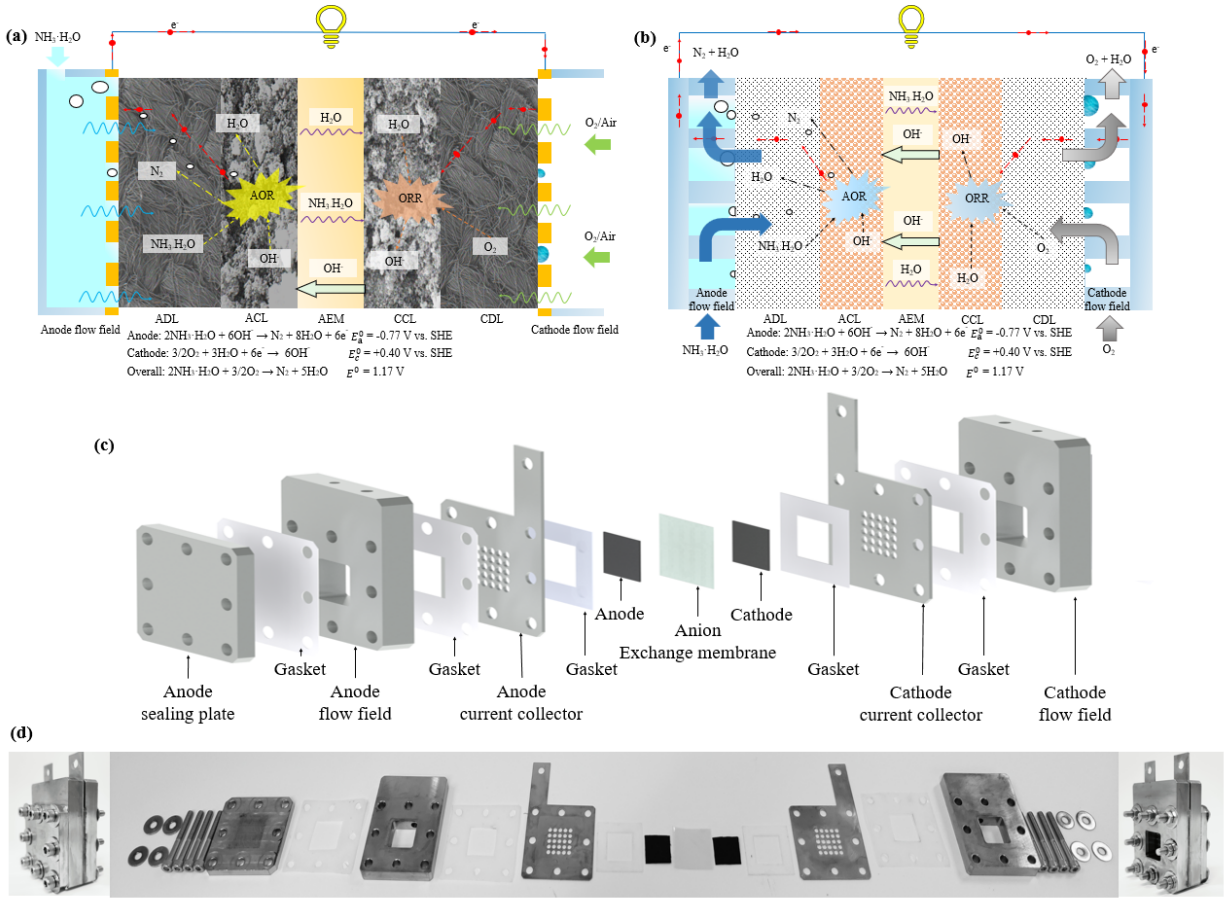

Fig. 1. (a) Working principle of passive direct ammonia fuel cells; (b) Working principle of active direct ammonia fuel cells; (c) Schematic diagram of the different components of the passive direct ammonia fuel cell; (d) Configuration of a passive direct ammonia fuel cell prototype.

The working principle of the passive ammonia fuel cell is shown in Fig. 1a. The developed passive ammonia fuel cell converts the chemical energy in ammonia into electrical energy through an electrochemical reaction. At the anode, the anolyte (including ammonia and potassium hydroxide) is injected into the anode flow field such that the ammonia solution fills the entire anode chamber. Here, KOH is added to improve the ionic conductivity of the anolyte and to ensure sufficient reactants for the anode reaction. The concentration gradient then drives the ammonia diffusion through the small holes of the anode collector towards the anode diffusion layer (ADL) and further into the ACL. At the ACL, ammonia and OH^- undergo an oxidation reaction to produce nitrogen and water and then release electrons. The equation for this reaction is as follows [25]:

$$2NH_3 \cdot H_2O + 6OH^- \rightarrow N_2 + 8H_2O + 6e^- \quad E_a^0 = -0.77 \text{ V vs. SHE} \tag{1}$$

Nitrogen gas, a product of the anode reaction, diffuses backwards from the CCL to the cathode diffusion layer (CDL) and then reaches the anode chamber and exits through the anode chamber outlet. In addition, the potential difference between the anode and cathode drives the migration of electrons, which are released by the ammonia oxidation reaction (AOR), from the anode to the cathode. However, as the membrane in the middle of the cell is insulating, electrons can only migrate from the anode to the cathode via an external circuit. Secondly, the pressure and concentration difference between the two sides of the anion exchange membrane (AEM) and the permeability of the membrane allows water and ammonia molecules on the anode side to be transported across the membrane to the cathode. The cathode flow field is designed as a self-breathing structure where the oxygen required for the oxygen reduction reaction (ORR) occurring on the catalyst layer of the cathode is obtained directly from the air, which is supplied by a vent directly connected to the open space in the cathode chamber. At the cathode, oxygen combines

with electrons from the anode and with water to form OH^-. The equation for this reaction is as follows [26]:

$$3/2O_2 + 3H_2O + 6e^- \rightarrow 6OH^- \qquad E_c^0 = +0.40 \text{ V vs. SHE} \tag{2}$$

The overall reaction of the cell is therefore given as follows:

$$2NH_3 \cdot H_2O + 3/2O_2 \rightarrow N_2 + 5H_2O \qquad E^0 = 1.17 \text{ V} \tag{3}$$

As shown in Fig. 1a, the OH^- produced at the cathode migrates across the membrane from the cathode to the anode and thus form an ionic flux. The driving force for the transport of OH^- across the membrane is the electric field force. As electrons migrate from the ACL to CCL, the anode become electropositive due to the loss of electrons, while the cathode is electronegative due to the gain of electrons. Thus, an electric field exists between the cathode and the anode. Since the carrier OH^- is negatively charged, it is subject to an electric field force in a direction from the cathode towards the anode. The ion flow (mainly OH^-) inside the membrane is therefore from the cathode to the anode. In addition, the ammonia in the anolyte is driven by the concentration gradient to diffuse to the cathode, where it is oxidized at the cathode. This results in both a waste of anode fuel and a reduction in the overall cell voltage, as ammonia oxidation at the cathode generates a mixed potential, thus reducing the overall cell voltage. Unlike conventional active ammonia fuel cells, passive ammonia fuel cells have a single injection of both fuel and oxidant, thus avoiding the need for complex and redundant supply systems. This could broaden the scenario for ammonia fuel cells in future renewable energy storage and applications. Furthermore, due to the absence of an active supply system and the typical flow field (Fig. 1b), the mass/charge mechanism within the passive ammonia fuel cell, such as the driving force, transport path, and efficiency of the mass transfer, changes accordingly.

3. Methods

3.1 Preparation of a membrane electrode assembly

In this work, membrane electrode assembly (MEA), the core component of the passive ammonia fuel cell includes the anode, the cathode, and the AEM separating the cathode and the anode. The anode is made up of an ADL and an ACL. The catalyst material used in the ACL is PtRu/C, where the mass fraction of PtRu is 60 wt.% and the atomic ratio of Pt to Ru is 1:1. The total loading of the precious metal catalyst in the anode electrode is 4.50 mg cm^{-2}. The ADL is carbon cloth, manufactured by Shanghai Hesen Company, HCP330N, with a thickness of approximately 290 μm. The preparation of the anode was described in detail in [21]. After the anode has been prepared, the overall thickness of the electrode is approximately 350 μm. Similar to the anode, the cathode also consists of a CCL and a CDL. The catalyst used in the CCL is Pd/C, with a mass fraction of 60 wt. % Pd and the loading of Pd in the cathode is 2.0 mg cm^{-2}. In addition, the CDL is also made of carbon cloth, the same type as the anode. It should be noted that the AEM used in this study is a Fumasep FAS-30, approximately 30 μm thick, purchased from Fuel Cell Store, U.S.A. The AEM was treated prior to the experiments in order to replace the internal anion channels with OH^- ion channels by the following procedure: the AEM was first immersed in 1.0 M KOH solution for 24 hours to form OH^- ion channels inside the membrane [27–29]. The membrane was then taken out of the alkaline solution and soaked in deionized water to remove any possible contaminants.

3.2 Experimental setup

The components of the developed passive ammonia fuel cell prototype are shown in Fig. 1c and Fig. S3. Within the anode compartment are components such as the sealing plate, gasket, anode

flow field, anode collector, and anode electrode. The anode sealing plate and two sealing gaskets near the anode flow field are designed to prevent leakage of the anolyte. In this study, the flow field and the collector are integrated, as shown in Fig. S4. The flow field of the developed fuel cell consists of small holes (approx. 3.2 mm in diameter) in the current collector, thus allowing the diffusion of fuel or oxidant into the catalyst layer. Regarding the open ratio of the flow field, when its value is too small, it is not conducive to the transfer of the anode fuel and the efficient supply of oxygen to the cathode. Therefore, increasing the open ratio facilitates mass transport [30]. However, when the open ratio is too large, the area within the flow field for the conduction of electrons is relatively reduced. As a result, 50% was chosen as the open ratio in this work. Besides, considering the effective area of the fuel cell, the larger the effective area, the greater the total power output. However, the excessive area can lead to high internal resistance and non-uniform mass transfer [27]. For this reason, an effective electrode area of 2.0×2.0 cm^2 was chosen. During the experiment, the anolyte, consisting of a mixture of ammonia and KOH in different concentrations, is injected into the inner chamber of the anode flow field plate in one shot. The ammonia in the anode flow field then diffuses through the small holes of the anode collector to reach the ADL and further transported to the ACL by concentration difference. The gasket between the anode collector and the anode electrode is mainly used to prevent leakage of the anolyte from the surrounding anode electrode (due to the porous structure of the anode electrode). The flow field on the cathode side is directly connected to the outside air, as the cathode needs to use the oxygen in the air directly as oxidant. As shown in Fig. 1d, the cathode side consists mainly of the open cathode flow field plate, the gasket, the cathode current collector and the cathode electrode. The fundamental principle of operation is that air from the open cathode flow field, which contains approximately 21% oxygen, diffuses through the small holes of the cathode current collector to

the CDL and then transferred to the CCL where ORR takes place. In this work, the anolyte is heated indirectly by heating the fuel cell unit using an additional heating device (heating rod) and the temperature is measured by thermocouples. The fuel cell performance tests are carried out by Arbin BT2000 (Arbin Instrument Inc.). In addition, the internal resistance of the fuel cell is measured by the resistance measurement procedure coupled in the Arbin BT2000 [31,32]. Besides, the Electrochemical impedance spectroscopy (EIS) is tested with a CHI 660E electrochemical workstation (Shanghai Chenhua Co., China). The surface morphology of electrode was observed using scanning electron microscopy (SEM) (Zeiss Sigma 300, Germany). Further details are included in the method section of the supporting information.

4. Results and discussion

4.1 General performance

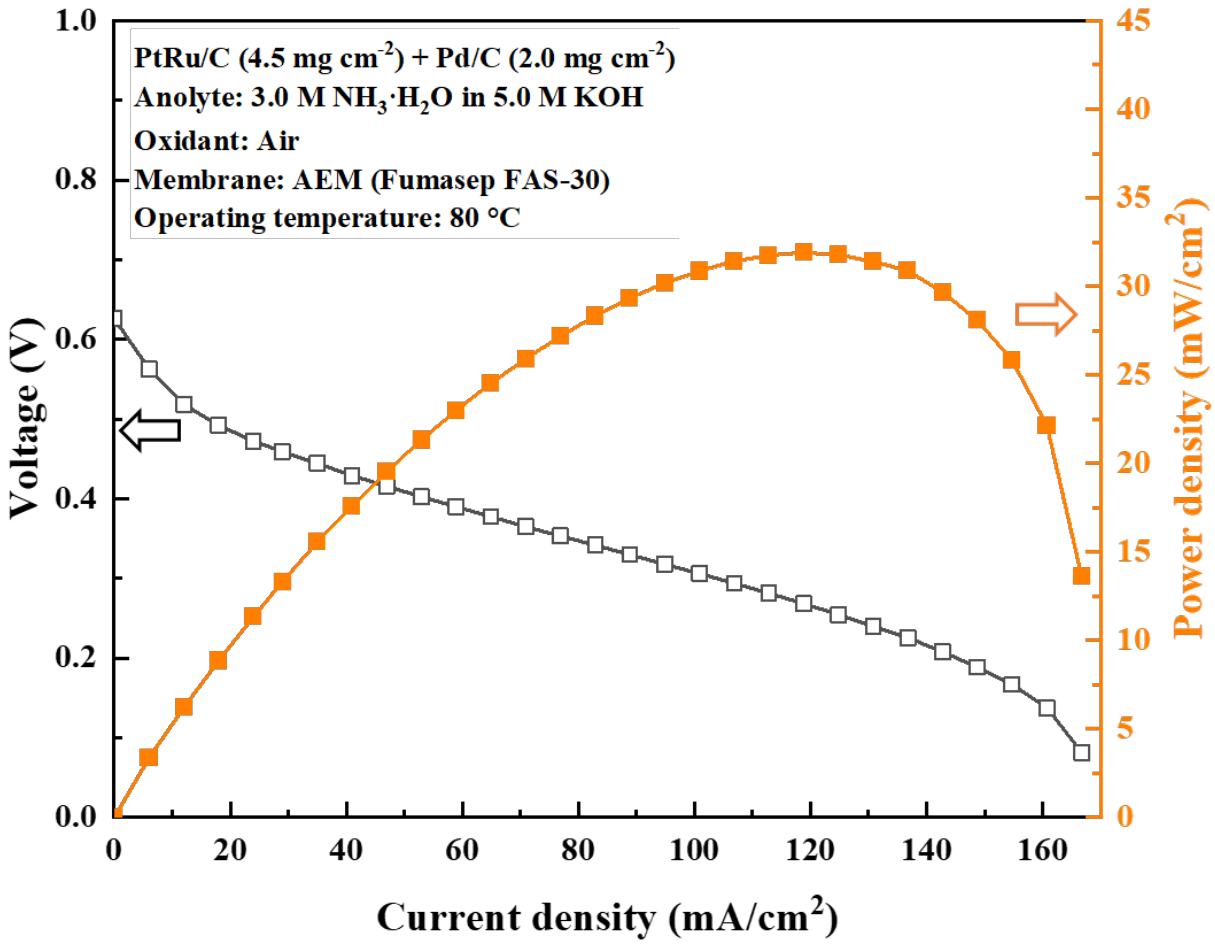

Fig. 2. Experimental results of the general performance of the passive ammonia fuel cells.

The passive ammonia fuel cell developed in this work consists of an anode, a cathode, and a membrane separating the cathode and the anode. The catalyst material for the anode is PtRu/C with a catalyst loading of 4.50 mg cm^{-2}, the catalyst used for the cathode is Pd/C with a catalyst loading of 2.0 mg cm^{-2} and the AEM used is Fumasep FAS-30 with a thickness of around 30 μm. As shown in Fig. 2, the OCV of this passive ammonia fuel cell is 0.63 V at an operating

temperature of 80 ℃, a drop of approximately 0.5 V relative to the theoretical voltage of 1.17 V. This voltage loss is mainly due to the overpotential loss from the AOR at the anode and the ORR at the cathode [18]. In addition, as the ammonia at the anode diffuses across the membrane to the cathode, it will be oxidized at the cathode, generating a mixed potential, further reducing the cell voltage [33]. As can be seen in Fig. 2, the polarization loss of fuel cell performance mainly consists of activation loss in the low current density region (0 - 20 mA cm^{-2}), ohmic loss in the medium current density region (20 - 140 mA cm^{-2}), and concentration loss in the relatively high current density region (140 - 165 mA cm^{-2}). Among them, the ohmic loss is the main cause for the degradation of the cell performance. In summary, the cell exhibits a peak power density of 31.9 mW cm^{-2}, which is higher than the performance of most passive fuel cells reported in the literature (see Table S1), and the maximum discharge current density achieved by the developed passive ammonia fuel cell is approximately 165 mA cm^{-2}.

4.2. Effects of various KOH concentrations and ammonia concentrations.

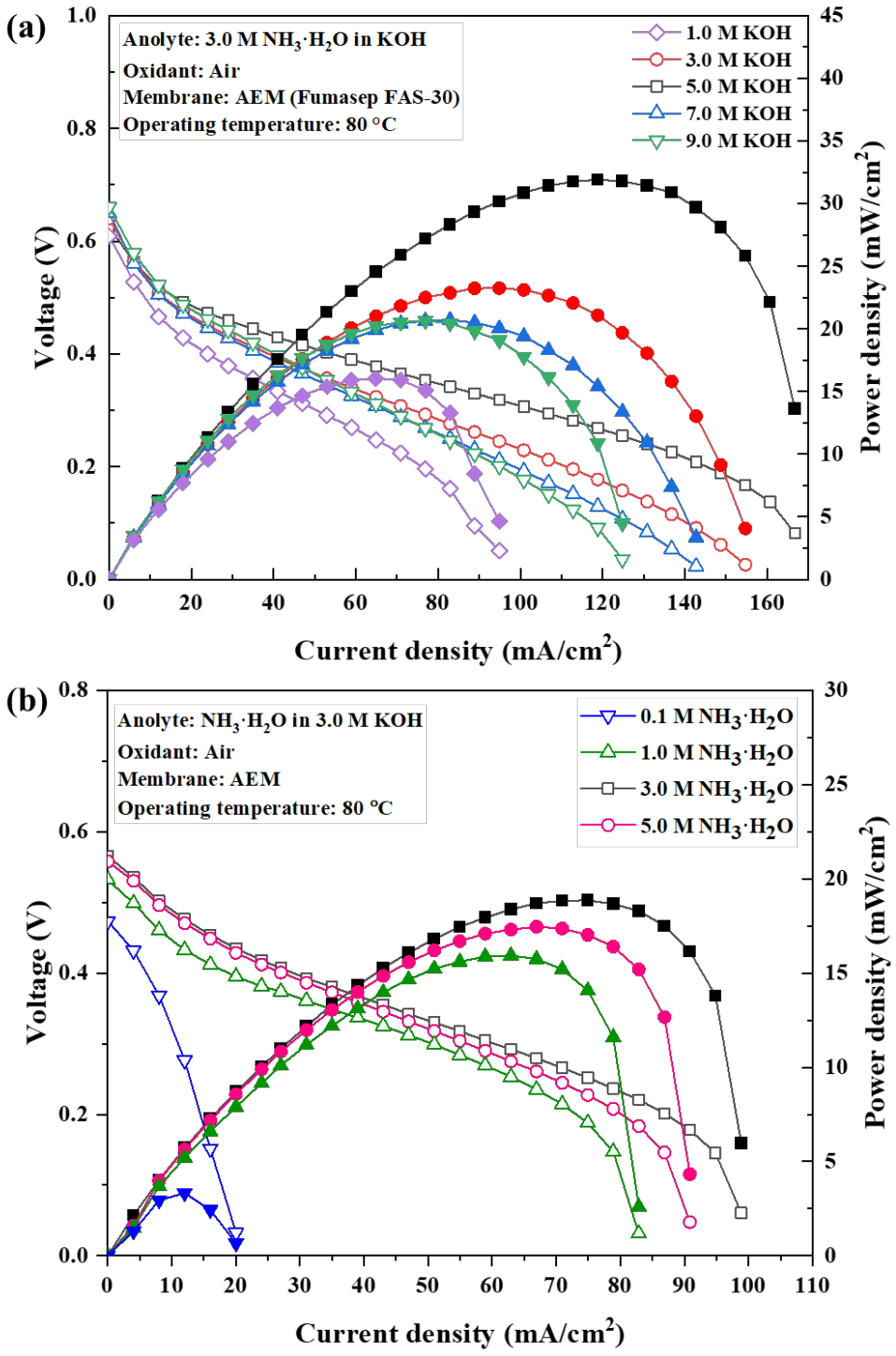

Fig. 3. Effect of reactants concentration (a) various KOH concentrations (1.0 M to 9.0 M); and (b) various ammonia concentrations (0.1 M to 5.0 M) on the fuel cell performance.

Different concentrations of KOH were investigated to determine their effect on the performance of the passive ammonia fuel cell and the experimental results are shown in Fig. 3. Firstly, it is straightforward to see that the OCV of the cell gradually increases from around 0.60 V to 0.66 V as the KOH concentration increases from 1.0 M to 9.0 M. The increase in the cell OCV can be attributed to the increase in the OH^- concentration in the anolyte. More specifically, when the OH^- concentration in the anolyte increases, the corresponding OH^- concentration on the ACL increases, resulting in more OH^- present on and near the catalyst surface, which facilitates the occurrence of the AOR at the anode, thus reducing the overpotential of the AOR [34]. Furthermore, it can be seen that the maximum discharge current density increases with increasing KOH concentration, from 90 mA cm^{-2} to approximately 160 mA cm^{-2}. Following the results of Fig. S5a, it was observed that as the concentration of KOH increases from 1.0 M to 5.0 M, the reaction kinetics of ammonia oxidation gradually increase. Meanwhile, the resistance of the electrolyte and electrode gradually decreases. Consequently, the corresponding peak power density also increases rapidly. However, when the KOH concentration was further increased from 5.0 M to 9.0 M, the peak power density of the fuel cell started to decrease. The main reason for this decrease in performance is due to the high concentration of KOH in the anolyte, which leads to the excessive viscosity of the anolyte, affecting the mobility of the species in the anolyte and particularly reducing the OH^- migration rate, which manifests externally as an increase in the internal resistance of the cell [35]. This can be verified in the experimental results in Fig. 3a, where the slopes of the polarization curves (blue and green lines) corresponding to 7.0 M KOH and 9.0 M KOH in the ohmic loss region are significantly higher than the slopes of the polarization curves (black lines) corresponding to 5.0 M KOH. Besides, the EIS results in Fig. S5-a show that the resistances of 7.0 M and 9.0 M KOH are slightly higher than that of 5.0 M, while the corresponding AOR kinetics are slower than that of

5.0 M KOH. In summary, the best cell performance was achieved at a KOH concentration of 5.0 M, with a peak power density of 31.9 mW cm^{-2}.

The effect of ammonia concentration on the fuel cell performance was investigated and the results are shown in Fig. 3b. Firstly, it can be seen that at a concentration of 0.1 M ammonia, the developed passive ammonia fuel cell exhibits severe concentration polarization and the voltage drops dramatically, such that the maximum current density of the cell is approximately 20 mA cm^{-2}. The reason for this occurrence is that as the discharge current density gradually increases, the ammonia consumption rate by the AOR on the ACL gradually increases [36,37]. Due to the low concentration of ammonia in the anolyte, the supply rate of ammonia from the anode chamber through the ADL to the ACL is limited and therefore cannot meet the consumption rate of ammonia on the ACL, resulting in concentration polarization in the cell. Secondly, as the ammonia concentration increases from 0.1 M to 3.0 M, the OCV of the cell continues to rise. This is attributed to the increase of ammonia concentration in the anolyte, which result to an increase in the concentration of ammonia on the ACL. The overpotential of the AOR at anode can therefore be reduced due to the presence of more ammonia on and near the catalyst surface. As a result, the corresponding peak power density of the developed fuel cell gradually increases as the ammonia concentration increases. A peak power density of approximately 20 mW cm^{-2} was achieved when the ammonia concentration was increased to 3.0 M. In accordance with the results of EIS test for different ammonia concentrations (Fig. S5-b), the resistance value was gradually reduced when the ammonia concentration increased from 0.1 M to 3.0 M with a slightly improvement of the reaction kinetics. However, when the ammonia concentration was further increased to 5.0 M, a small increase in the resistance value was observed. Meanwhile, the OCV of the cell decreased slightly, which resulted in a decrease of the peak power density of the fuel cell. The reasons for

the decline in fuel cell OCV are as follows: since the AEM used in the fuel cells is a porous layer structure, it allows water molecules to pass through. Ammonia (NH_3), which is present in the form of aqueous solution ($NH_3 \cdot H_2O$) in the anolyte, can transfer from the anode to the cathode along with water through the membrane. However, when the ammonia reaches the cathode, as Pd/C is applied as the cathode electrocatalyst, AOR will also occur on the cathode, releasing electrons and thus generating a mixed potential, which in turn leads to a reduction in the overall voltage of the fuel cell and affects its performance [21]. Consequently, when the ammonia concentration is increased from 3.0 M to 5.0 M, more ammonia crossover to the cathode of the fuel cell, thus exacerbating the crossover phenomenon and generating more mixed potential, which in turn causes voltage drop of the fuel cell.

4.3. Effects of operating temperature and membrane thickness

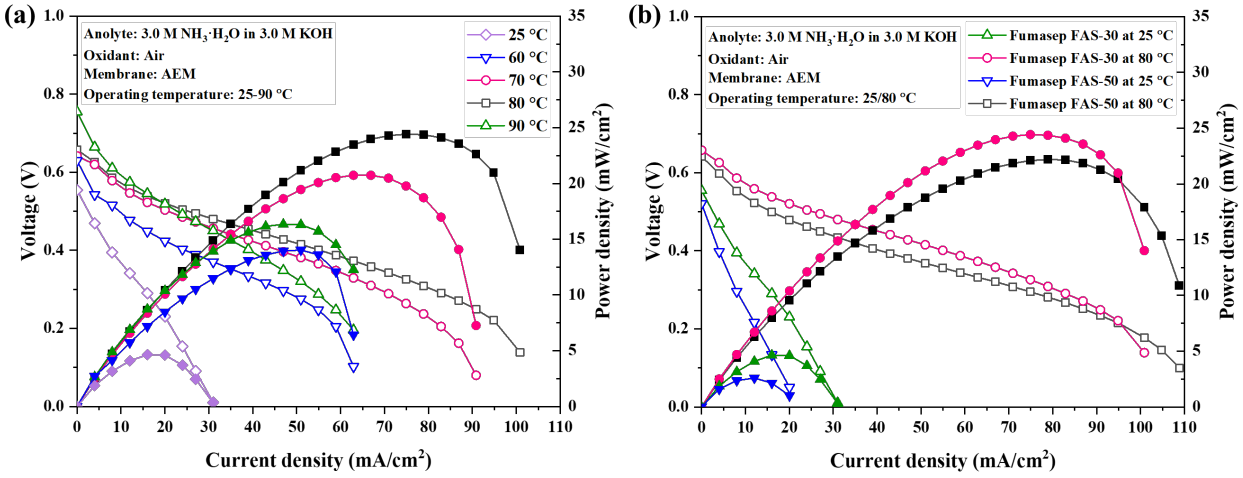

Fig. 4. (a) Performance comparison of the fuel cell at different operating temperatures (25 to 90 °C); (b) Effect of the thickness of the AEM on fuel cell performance.

A range of temperatures (25, 60, 70, 80, and 90 °C) were tested to investigate the effect of operating temperature on the performance of the fuel cell. It can be seen from Fig. 4a. that the performance

of the fuel cell increases as the operating temperature increases from 25 to 80 °C. The reasons for the enhanced performance of the fuel cell are as follows: firstly, the reaction kinetics of AOR at the anode and ORR at the cathode are accelerated by the increase in temperature, thus reducing the activation polarization losses in the low current density region [21]. Following the analysis in Fig. S6 and Fig. S7, it can be concluded that there is a 20% reduction in activation losses for fuel cell operation at 80 °C (52.2%) compared to activation losses (Fig. S8) at 25 °C (70.9%). Secondly, at room temperature, the mass transport within a passive ammonia fuel cell primarily relies on concentration gradient driven by diffusion and natural convection, which results in slower mass transport compared to the active fuel supply method. However, as the operating temperature rises, this results in an acceleration of the reactants and ion transport within the fuel cell electrodes as well as the membrane, resulting in a dramatic reduction in the overall internal resistance of the cell. It can be seen from Fig. S9 that the cell resistance reduced from 0.689 Ω cm^2 to 0.185 Ω cm^2 when the operating temperature increased from 25 to 80 °C. However, as the operating temperature increases from 80 °C to 90 °C, the performance of the fuel cell decreases. This is due to the fact that the higher operating temperature reduces the water content in the anion exchange membrane, which increases the internal resistance of the cell (from 0.185 Ω cm^2 at 80 °C to 0.431 Ω cm^2 at 90 °C), resulting in a decrease in overall cell performance. As a result, 80 °C would be an ideal operating temperature for the developed fuel cell.

The performance of membranes thicknesses at different temperatures was tested and the experimental results are shown in Fig. 4b. It can be seen that Fumasep FAS-30 (~30 μm) has a higher peak power density than Fumasep FAS-50 (~50 μm) membranes at the same operating temperature. The reason for the better performance achieved by a thinner membrane is that the transport path within the membrane is shorter. As mentioned earlier, OH^- inside the passive

ammonia fuel cell is transported across the membrane from the cathode to the anode, driven by electric field forces. When the transport path is shorter, the transport of the hydroxide ions becomes relatively easy and thus the resistance of the fuel cell is reduced [26]. In addition, the ORR that occurs at the cathode of a passive ammonia fuel cell requires water as a reactant, which comes from the diffusion of water across the membrane from the anolyte. Therefore, when the membrane thickness is thinner, the diffusion of water molecules is also facilitated, thus promoting the ORR at the cathode.

4.4 Effects of various anode catalyst loading.

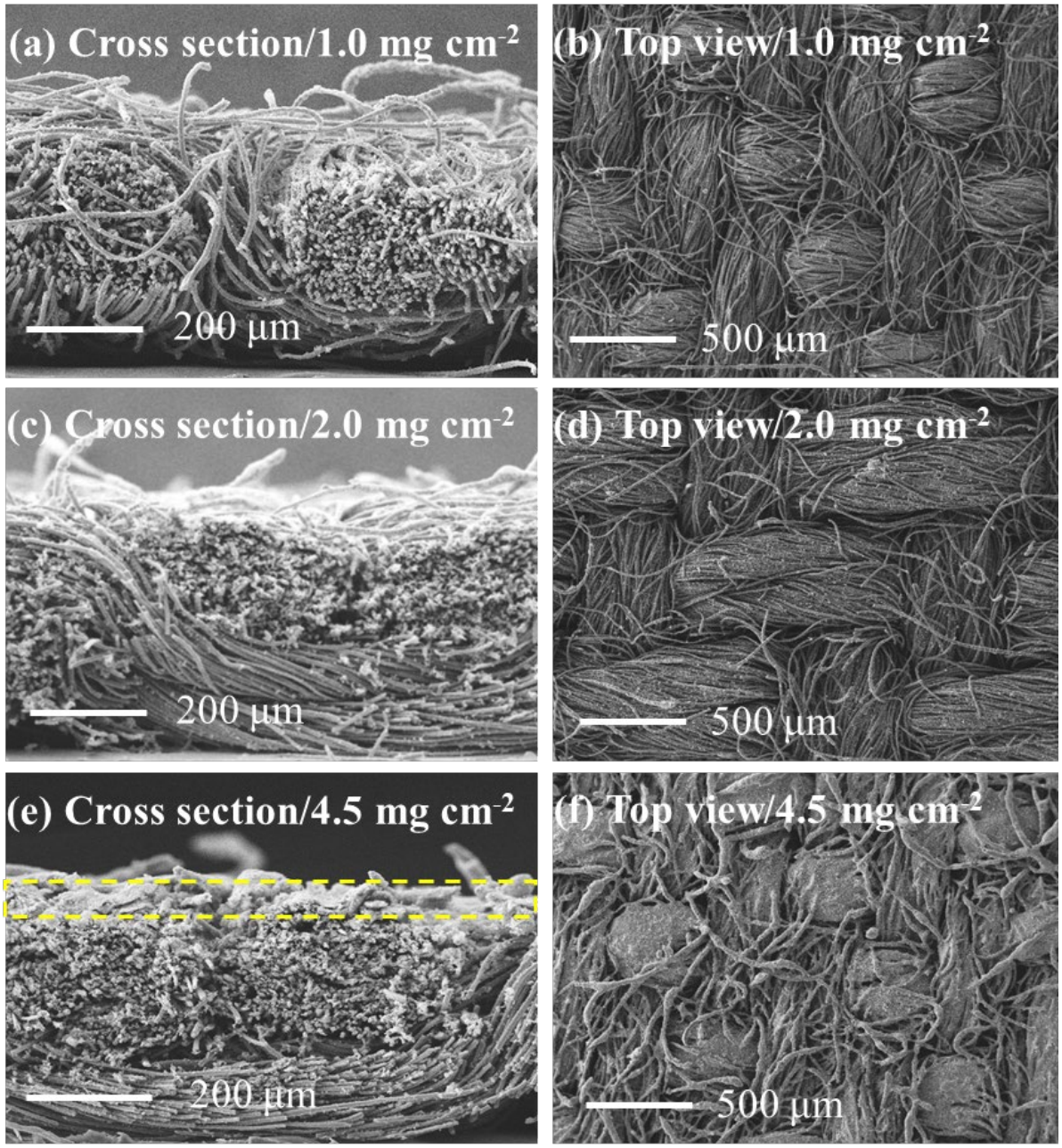

Fig. 5. Material characterization results for various anode catalyst (PtRu/C) loadings: (a) 1.0 mg cm^{-2} of cross section view; (b) 1.0 mg cm^{-2} of top review; (c) 2.0 mg cm^{-2} of cross section view; (d) 2.0 mg cm^{-2} of top review; (e) 4.5 mg cm^{-2} of cross section view; (f) 4.5 mg cm^{-2} of top review.

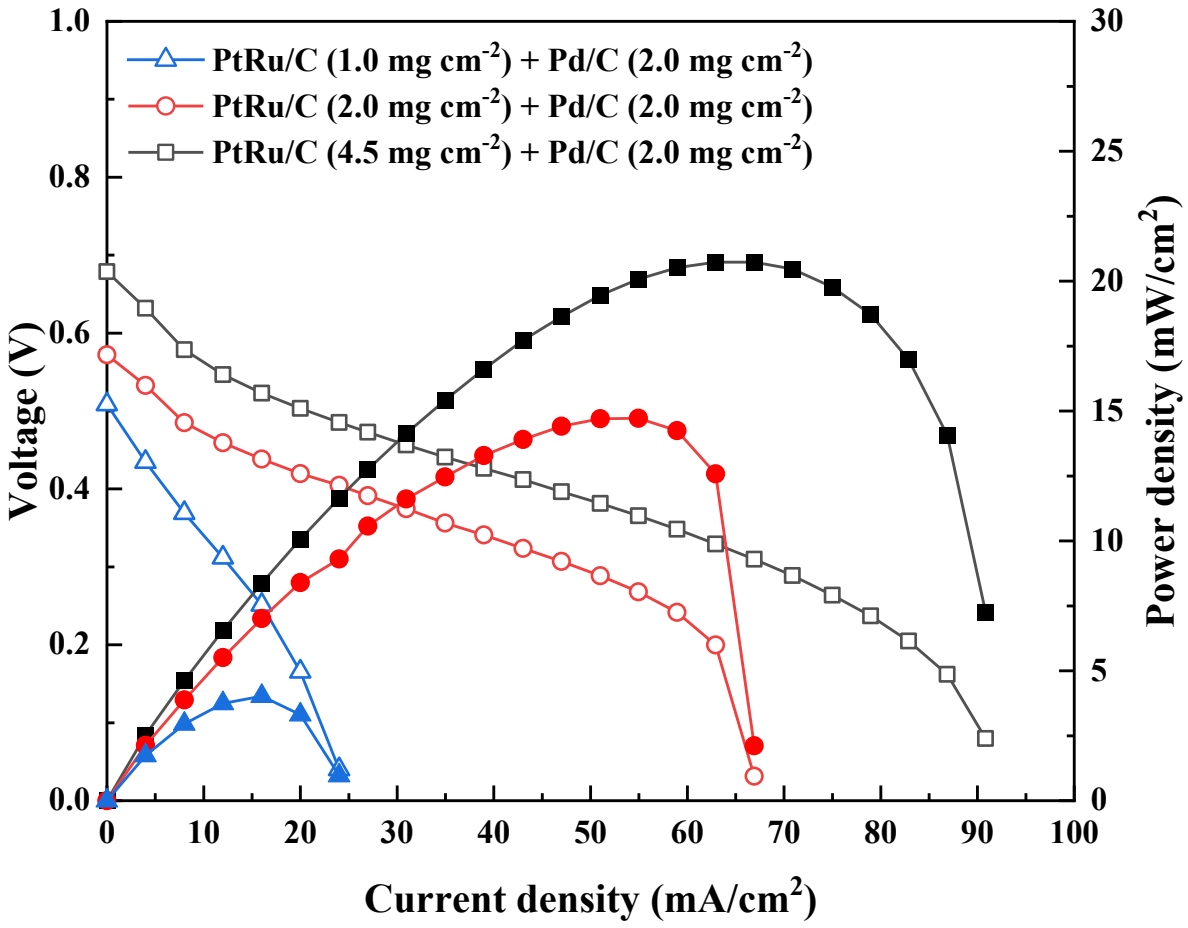

Fig. 6. Performance comparison of various anode catalyst loading from 1.0 mg cm^{-2} to 4.5 mg cm^{-2}.

The material characterization of the anodes with different catalyst loadings was first carried out and the results are shown in Fig. 5. According to the cross-sectional morphology, when the catalyst loading is 1.0 and 2.0 mg cm^{-2}, it can be seen that no obvious catalyst layer structure is formed on the surface of the diffusion layer (Fig. 5a-d). The main reason is because of the use of carbon cloth (HCP330N) for the ADL of the passive ammonia fuel cell. Due to the large pore size of the carbon cloth (ranging from tens to hundreds of microns) [38], the anode catalyst (particles in the nanometer range in diameter) easily escapes from the surface of the carbon cloth to the interior of the diffusion layer, thus reducing the amount of catalyst on the surface of the carbon cloth. When

the catalyst loading is increased to 4.5 mg cm^{-2}, a catalyst layer with a thickness of about 20-40 μm is observed (Fig. 5e and Fig. 5f). This can also be verified from the top view, where no catalyst is evident on the surface of the diffusion layer when the catalyst loading is 1.0 mg cm^{-2}. In contrast, when the catalyst loading was increased to 4.5 mg cm^{-2}, the presence of a layer structure on the surface of the diffusion layer is evident. The effect of the anode catalyst loading on the cell performance was then investigated and the experimental results are shown in Fig. 6. It can be seen that the cell performance increases with increasing catalyst loading. The performance enhancement consists of several factors: firstly, as the catalyst loading increases, there are more active sites on the electrode for electrochemical reactions. As a result, more triple-phase interfaces can be constructed within the electrode (consisting of the catalyst nanoparticle-solid phase, the ammonia and OH^- in the electrolyte-liquid phase, and the nitrogen-gas phase), resulting in a lower overpotential for the AOR and thus making it easier for the AOR to occur. Secondly, as the noble metal catalyst loading increases, the overall conductivity of the cell also increases, which facilitates the conduction of electrons and thus also reduces internal resistance and ohmic losses, thus improving the cell performance.

4.5 Effects of hydrophilic/hydrophobic diffusion layer

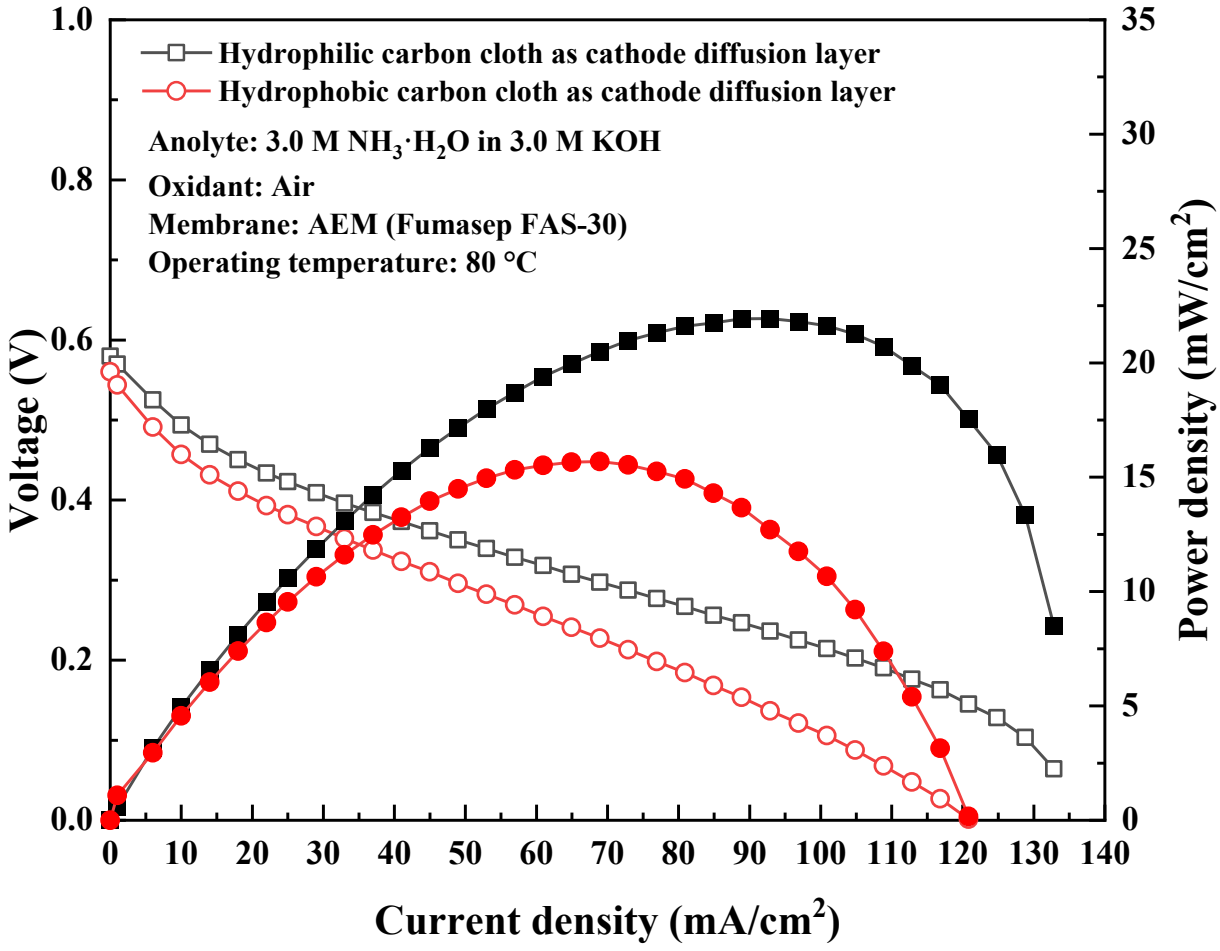

Fig. 7. Effect of hydrophilicity and hydrophobicity of the cathode diffusion layer on fuel cell performance.

The effect of using hydrophilic and hydrophobic CDL on the cell performance is investigated in this section. The experimental results are shown in Fig. 7 and it can be seen that when the cell is operated with a hydrophilic CDL, it exhibits higher power density. The reason for this phenomenon is that the passive ammonia fuel cell using hydrophobic carbon cloth as the CDL has a larger area-specific resistance compared with the cell using hydrophilic carbon cloth as the CDL. To clearly explain the reasons for the increased internal resistance of the cell, a schematic diagram

of the water content of the main components inside the fuel cell is displayed (Fig. S10) as a way of demonstrating the difference between using hydrophilic and hydrophobic CDL. The main source of water molecules in a passive ammonia fuel cell is the anolyte. The water molecules in the anolyte will enter the ADL driven by a concentration gradient, and then diffuse into the ACL. As the AEM is permeable to water, water molecules that reach the ACL can penetrate the AEM and transport to the cathode, where the water reach the CCL and participate in the ORR. Theoretically, as the ORR on the cathode requires the participation of water molecules, the greater the number of water molecules, the more favorable the ORR will be. However, according to Fig. 5c, at a catalyst loading of 2.0 mg cm^{-2}, there is no visible catalytic layer on the surface of the diffusion layer. In other words, the CCL is very thin and almost blends in with the diffusion layer. When excess water reaches the cathode side, the water molecules on the CCL enter the CDL due to the concentration difference drive and capillary forces. As the oxidant on the cathode side of the passive ammonia fuel cell is completely dependent on the natural convection in the air from the open cathode structure, the water molecules remaining in the porous structure in the CDL could block the oxygen transport path on the cathode side (this phenomenon is also known as water flooding) [39]. This will prevent the oxygen from reaching the CCL in time, thereby affecting the ORR on the CCL and thus the overall performance of the fuel cell. It is therefore extremely important to balance the water content on the cathode side. When using a hydrophobic diffusion layer, the hydrophobic surface on the CDL can directly contact the AEM due to the small thickness of the CCL, thus reducing the water contents near the interface between the membrane and the CDL (see Fig. S10-a), which can increase the internal resistance of the cell and reduce the cell performance [40]. This problem can be avoided when using hydrophilic carbon cloth as a CDL (Fig. S10-b), which ensures that the water content near the interface is relatively high. Furthermore,

it can be observed that the OCV of the cell (~0.6 V) with the hydrophilic carbon cloth is close to that of the cell when hydrophobic carbon cloth is used. Meanwhile, no water was observed on the outer surface of the cathode side during the experimental operation, indicating that the utilization of the hydrophilic diffusion layer will not result in significant water flooding. In summary, better performance can be achieved by using hydrophilic carbon cloth as the cathode diffusion layer.

4.6 Durability test

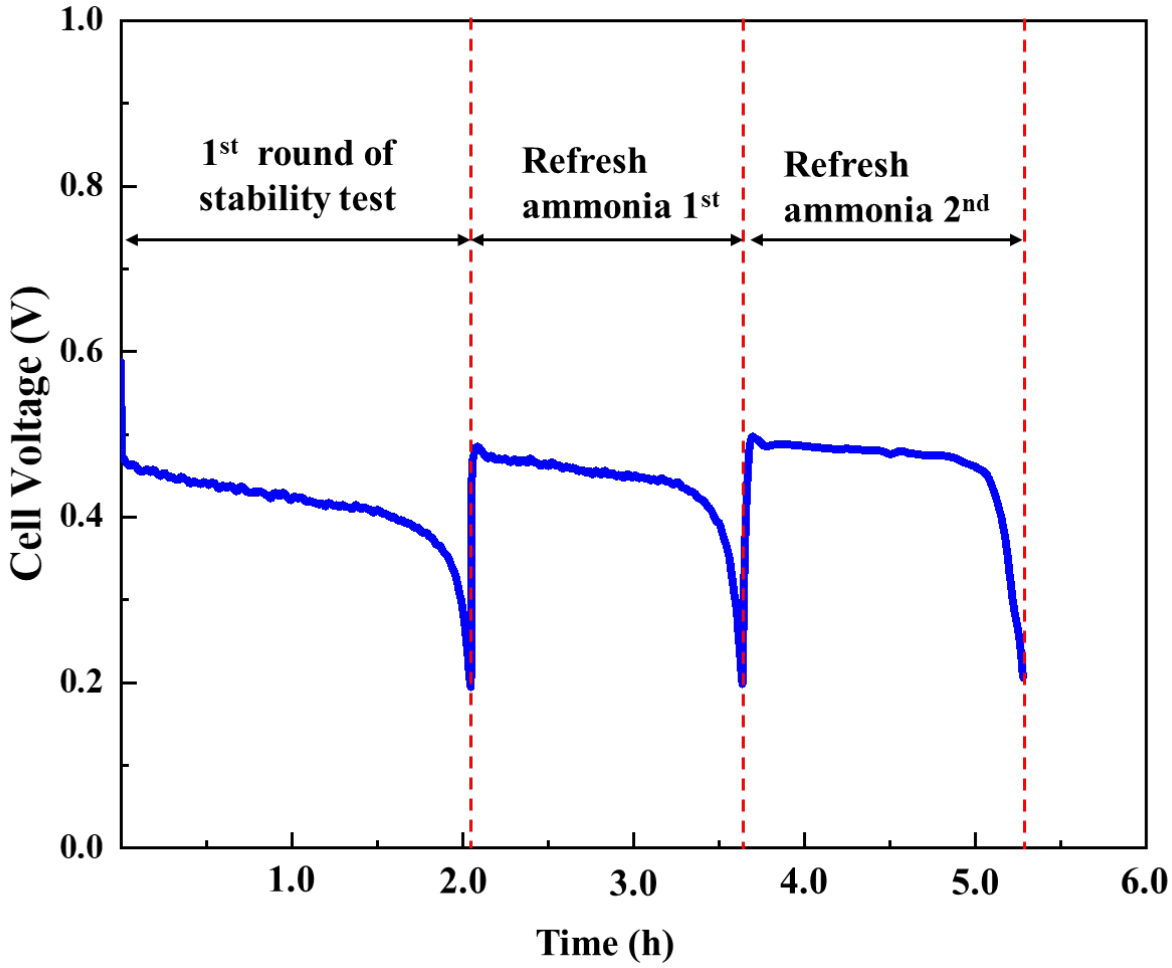

Fig. 8. Experimental results of fuel cell stability test and refreshing ammonia: continuous discharge at a current density of 10.0 mA cm^{-2}.

The stability of the passive ammonia fuel cell is investigated and the results are shown in Fig. 8. The results show that the developed passive ammonia fuel cell can maintain the cell voltage for approximately 2.0 hour in a constant current discharge test at a current density of 10.0 mA cm^{-2}. The reasons for this phenomenon are as follows: at the beginning of the cell operation, due to the sufficient concentration of ammonia in the anolyte, the ammonia in the anode chamber enters the ADL through the small holes in the anode current collector and then diffuses through the diffusion

layer to the ACL. At this point, the rate of ammonia consumption on the catalyst layer by AOR is also constant, as the cell is under a constant current discharge condition. Since the ammonia is consumed on the catalyst layer, the instantaneous concentration of ammonia in the adjacent ADL and anode chamber is higher than the concentration of ammonia in the ACL. The driving force generated by the difference in concentration causes the ammonia in the ADL and anode chamber to diffuse towards the ACL, replenishing the ammonia consumed by the AOR. When the rate of ammonia consumption in the ACL is balanced with the rate of ammonia supply from the ADL and the anode chamber, the cell voltage is maintained at a steady state. If the rate of ammonia consumption in the ACL is higher than the rate of ammonia supply, the cell voltage drops. After 1.5 hour, the cell voltage starts to decline and at 1.75 h the cell voltage starts to drop drastically. The main reason is that the ammonia concentration in the ACL is too low for the rate of ammonia consumption, thus causing a sharp drop in the cell voltage. To further verify the stability of the fuel cell, the effect of supplying fresh ammonia to the anode side is tested (Fig. 8) and results demonstrate that the fuel cell can continue to operate stably. It is worth noting that after refreshing the ammonia, the voltage of the fuel cell becomes slightly higher than when the fuel was first injected (during discharge state). The possible reasons are summarized as follows: Since the cell has been discharged during the refreshing of the ammonia, the fuel cell has reached a relatively stable state internally at this moment, and after refueling the ammonia, the OCV of the cell will be slightly higher than when it was first injected, and therefore will exhibit a slightly higher voltage at the same discharge current. In addition, it can also be observed that the constant current discharge time of the cell is reduced after refreshing the ammonia, which can be attributed to the slow performance degradation of the cell electrodes during operation.

5. Concluding remarks

In this work, a new passive ammonia fuel cell prototype was designed and tested, where the anolyte was passively supplied, eliminating the need for a complex fuel delivery system, while the cathode was designed as an open cathode, using oxygen from the ambient air directly as the oxidant. To demonstrate the working principle of fuel cell, its general performance was firstly investigated and the results showed that the developed fuel cell could provide a peak power density of 31.9 mW cm^{-2} and an open circuit voltage of 0.63 V. Secondly, the passive ammonia fuel cell prototype was tested under different operating conditions to gain insight into the physical and chemical processes involved in the cell, as well as to enhance understanding on the mass/charge transfer mechanisms. The results show that the operating temperature and the concentration of KOH in the anolyte exert significant effect on the anode AOR, which can significantly enhance the fuel cell performance. In addition, structural parameters of the membrane electrode assembly, such as the thickness of the membrane, catalyst loading, and hydrophobicity of the diffusion layer, were investigated and analyzed to understand their effects on the mass transport behavior, electrochemical reactions, and performance of the fuel cell. The results show that the use of thinner membranes can reduce the internal resistance of the cell by shortening the mass transfer path of OH^-. In addition, a higher catalyst loading allows for the construction of more triple-phase reaction interfaces on the ACL, thus improving the overall cell performance. Furthermore, a constant current discharge stability test was carried out, which showed that the fuel cell could be discharged stably for around 2.0 hours and continued to operate stably when refreshed with ammonia. Following these results, this work integrates cell prototype design and working principle analysis, as well as explores the effects of operating conditions and core component parameters on the mass/charge transport behavior and

their impacts on the cell performance, paving the way for further development of passive ammonia fuel cells.

Acknowledgement

The work described in this paper was supported by a grant from the National Natural Science Foundation of China (No. 52022003) and a grant from the Shenzhen Science and Technology Innovation Commission (No. SGDX20201103095204 04).

References

[1] A. Valera-Medina, H. Xiao, M. Owen-Jones, W.I.F. David, P.J. Bowen, Ammonia for power, Prog. Energy Combust. Sci. 69 (2018) 63–102.

[2] D.R. MacFarlane, P. V. Cherepanov, J. Choi, B.H.R. Suryanto, R.Y. Hodgetts, J.M. Bakker, F.M. Ferrero Vallana, A.N. Simonov, A Roadmap to the Ammonia Economy, Joule. 4 (2020) 1186–1205.

[3] S.S. Rathore, S. Biswas, D. Fini, A.P. Kulkarni, S. Giddey, Direct ammonia solid-oxide fuel cells: A review of progress and prospects, Int. J. Hydrogen Energy. 46 (2021) 35365–35384.

[4] G. Jeerh, M. Zhang, S. Tao, Recent progress in ammonia fuel cells and their potential applications, J. Mater. Chem. A. 9 (2021) 727–752.

[5] R.H. Dolan, J.E. Anderson, T.J. Wallington, Outlook for ammonia as a sustainable transportation fuel, Sustain. Energy Fuels. 5 (2021) 4830–4841.

[6] R. Chen, S. Zheng, Y. Yao, Z. Lin, W. Ouyang, L. Zhuo, Z. Wang, Performance of direct ammonia fuel cell with PtIr/C, PtRu/C, and Pt/C as anode electrocatalysts under mild conditions, Int. J. Hydrogen Energy. 46 (2021) 27749–27757.

[7] Y. Zhao, B.P. Setzler, J. Wang, J. Nash, T. Wang, B. Xu, Y. Yan, An Efficient Direct Ammonia Fuel Cell for Affordable Carbon-Neutral Transportation, Joule. 3 (2019) 2472–2484.

[8] M. Perčić, N. Vladimir, I. Jovanović, M. Koričan, Application of fuel cells with zero-carbon fuels in short-sea shipping, Appl. Energy. 309 (2022).

[9] X. Mao, J. Sang, C. Xi, Z. Liu, J. Yang, W. Guan, J. Wang, C. Xia, S.C. Singhal, Performance evaluation of ammonia-fueled flat-tube solid oxide fuel cells with different build-in catalysts, Int. J. Hydrogen Energy. 47 (2022) 23324–23334.

[10] F. Isorna Llerena, A. de las Heras Jiménez, E. López González, F. Segura Manzano, J.M. Andújar Márquez, Effects of Ammonia Impurities on the Hydrogen Flow in High and Low Temperature Polymer Electrolyte Fuel Cells, Fuel Cells. 19 (2019) 651–662.

[11] T. Wang, Y. Zhao, B.P. Setzler, Y. Yan, Improving Performance and Durability of Low Temperature Direct Ammonia Fuel Cells: Effect of Backpressure and Oxygen Reduction Catalysts, J. Electrochem. Soc. 168 (2021) 014507.

[12] K. Sato, S. Zaitsu, G. Kitayama, S. Yagi, Y. Kayada, Y. Nishida, Y. Wada, K. Nagaoka, Operando Spectroscopic Study of the Dynamics of Ru Catalyst during Preferential Oxidation of CO and the Prevention of Ammonia Poisoning by Pt, J. Am. Chem. Soc. 2 (2022) 1627–1637.

[13] M. Zhang, J. Zhang, G. Jeerh, P. Zou, B. Sun, M. Walker, K. Xie, S. Tao, A symmetric direct ammonia fuel cell using ternary NiCuFe alloy embedded in a carbon network as electrodes, J. Mater. Chem. A. (2022) 18701–18713.

[14] G. Jeerh, P. Zou, M. Zhang, S. Tao, Perovskite oxide LaCr0.25Fe0.25Co0.5O3-δ as an efficient non-noble cathode for direct ammonia fuel cells, Appl. Catal. B Environ. 319 (2022) 121919.

[15] Q. Shu, J. Zhang, B. Hu, X. Deng, J. Yuan, R. Ran, W. Zhou, Z. Shao, Rational Design of a High-Durability Pt-Based ORR Catalyst Supported on Mn/N Codoped Carbon Sheets for PEMFCs, Energy Fuels. 36 (2022) 1707–1715.

[16] H. Zhang, Y. Zhou, K. Pei, Y. Pan, K. Xu, Y. Ding, B. Zhao, K. Sasaki, Y. Choi, Y. Chen, M. Liu, An efficient and durable anode for ammonia protonic ceramic fuel cells, Energy Environ. Sci. 15 (2022) 287–295.

[17] S. Gottesfeld, The Direct Ammonia Fuel Cell and a Common Pattern of Electrocatalytic Processes, J. Electrochem. Soc. 165 (2018) J3405–J3412.

[18] T. Wang, Y. Zhao, B.P. Setzler, R. Abbasi, S. Gottesfeld, Y. Yan, A high-performance 75 W direct ammonia fuel cell stack, Cell Reports Phys. Sci. 3 (2022) 100829.

[19] Y. Aoki, T. Yamaguchi, S. Kobayashi, D. Kowalski, C. Zhu, H. Habazaki, High-Efficiency Direct Ammonia Fuel Cells Based on BaZr 0.1 Ce 0.7 Y 0.2 O 3− δ /Pd Oxide-Metal Junctions , Glob. Challenges. 2 (2018) 1700088.

[20] P. Zou, S. Chen, R. Lan, S. Tao, Investigation of Perovskite Oxide SrCo0.8Cu0.1Nb0.1O3–Δ as a Cathode Material for Room Temperature Direct Ammonia Fuel Cells, ChemSusChem. 12 (2019) 2788–2794.

[21] Y. Liu, Z. Pan, O.C. Esan, X. Xu, L. An, Performance Characteristics of a Direct Ammonia Fuel Cell with an Anion Exchange Membrane, Energy Fuels. 36 (2022) 13203–13211.

[22] X. Shi, Y. Dai, O.C. Esan, X. Huo, L. An, T. Zhao, A Passive Fuel Cell Fed with an Electrically Rechargeable Liquid Fuel, ACS Appl. Mater. Interfaces. 13 (2021) 48795–48800.

[23] Z. Pan, Y. Bi, L. An, Performance characteristics of a passive direct ethylene glycol fuel cell with hydrogen peroxide as oxidant, Appl. Energy. 250 (2019) 846–854.

[24] X. Su, Z. Pan, L. An, Performance characteristics of a passive direct formate fuel cell, Int. J. Energy Res. 43 (2019) 7433–7443.

[25] O. Siddiqui, I. Dincer, A review and comparative assessment of direct ammonia fuel cells, Therm. Sci. Eng. Prog. 5 (2018) 568–578.

[26] R. Lan, S. Tao, Ammonia as a suitable fuel for fuel cells, Front. Energy Res. 2 (2014) 3–6.

[27] Z. Pan, Y. Bi, L. An, Performance characteristics of a passive direct ethylene glycol fuel cell with hydrogen peroxide as oxidant, Appl. Energy. 250 (2019) 846–854.

[28] S. Haj-Bsoul, J.R. Varcoe, D.R. Dekel, Measuring the alkaline stability of anion-exchange membranes, J. Electroanal. Chem. 908 (2022) 116112.

[29] L. An, T.S. Zhao, L. Zeng, X.H. Yan, Performance of an alkaline direct ethanol fuel cell with hydrogen peroxide as oxidant, Int. J. Hydrogen Energy. 39 (2014) 2320–2324.

[30] L. Wang, L. Yin, W. Yang, Y. Cheng, F. Wen, C. Liu, L. Dong, M. Wang, S. Ma, X. Feng, Evaluation of structural aspects and operation environments on the performance of passive micro direct methanol fuel cell, Int. J. Hydrogen Energy. 46 (2021) 2594–2605.

[31] D. Anseán, M. González, J.C. Viera, J.C. Álvarez, C. Blanco, V.M. García, Internal Resistance Analysis, IEEE Veh. Power Propuls. Conf. (2014) 0–5.

[32] H.G. Schweiger, O. Obeidi, O. Komesker, A. Raschke, M. Schiemann, C. Zehner, M. Gehnen, M. Keller, P. Birke, Comparison of several methods for determining the internal resistance of lithium ion cells, Sensors. 10 (2010) 5604–5625.

[33] Z.F. Pan, L. An, C.Y. Wen, Recent advances in fuel cells based propulsion systems for unmanned aerial vehicles, Appl. Energy. 240 (2019) 473–485.

[34] X. Su, Z. Pan, L. An, Ion Transport Characteristics in Membranes for Direct Formate Fuel Cells, Front. Chem. 8 (2020) 1–16.

[35] W. Jin, H. Du, S. Zheng, H. Xu, Y. Zhang, Comparison of the oxygen reduction reaction between NaOH and KOH solutions on a Pt electrode: The electrolyte-dependent effect, J. Phys. Chem. B. 114 (2010) 6542–6548.

[36] C. Xu, T.S. Zhao, Q. Ye, Effect of anode backing layer on the cell performance of a direct methanol fuel cell, Electrochim. Acta. 51 (2006) 5524–5531.

[37] Q.X. Wu, T.S. Zhao, R. Chen, W.W. Yang, A microfluidic-structured flow field for passive direct methanol fuel cells operating with highly concentrated fuels, J. Micromechanics Microengineering. 20 (2010).

[38] T.S. Zhao, C. Xu, R. Chen, W.W. Yang, Mass transport phenomena in direct methanol fuel cells, Prog. Energy Combust. Sci. 35 (2009) 275–292.

[39] C. Xu, A. Faghri, X. Li, T. Ward, Methanol and water crossover in a passive liquid-feed direct methanol fuel cell, Int. J. Hydrogen Energy. 35 (2010) 1769–1777.

[40] J. Lorenz, H. Janßen, K. Yassin, J. Leppin, Y.W. Choi, J.E. Cha, M. Wark, S. Brandon, D.R. Dekel, C. Harms, A. Dyck, Impact of the Relative Humidity on the Performance Stability of Anion Exchange Membrane Fuel Cells Studied by Ion Chromatography, ACS Appl. Polym. Mater. (2022).

Figures captions:

Fig. 1. (a) Working principle of passive direct ammonia fuel cells; (b) Working principle of active direct ammonia fuel cells; (c) Schematic diagram of the different components of the passive direct ammonia fuel cell; (d) Configuration of a passive direct ammonia fuel cell prototype.

Fig. 2. Experimental results of general performance of the developed passive ammonia fuel cells.

Fig. 3. Effect of reactants concentration (a) various KOH concentrations (1.0 M to 9.0 M); and (b) various ammonia concentrations (0.1 M to 5.0 M) on fuel cell performance.

Fig. 4. (a) Performance comparison of the fuel cell at different operating temperatures (25 to 90 °C); (b) Effect of the thickness of the AEM on fuel cell performance.

Fig. 5. Material characterization results for various anode catalyst (PtRu/C) loadings: (a) 1.0 mg cm^{-2} of cross section view; (b) 1.0 mg cm^{-2} of top review; (c) 2.0 mg cm^{-2} of cross section view; (d) 2.0 mg cm^{-2} of top review; (e) 4.5 mg cm^{-2} of cross section view; (f) 4.5 mg cm^{-2} of top review.

Fig. 6. Performance comparison of various anode catalyst loading from 1.0 mg cm^{-2} to 4.5 mg cm^{-2}.

Fig. 7. Effect of hydrophilicity and hydrophobicity of the cathode diffusion layer on fuel cell performance.

Fig. 8. Experimental results of fuel cell stability test and refreshing ammonia: continuous discharge at a current density of 10.0mA cm^{-2}.